HHS Public Access

Author manuscript

J Unmanned Veh Syst. Author manuscript; available in PMC 2019 August 09.

Published in final edited form as:

J Unmanned Veh Syst. 2017 December ; 5(4): 146–158. doi:10.1139/juvs-2016-0019.

Spectroscopic Analysis for Mapping Wildland Fire Effects from Remotely Sensed Imagery

Dale Hamilton, M.S. [Assistant Professor of Computer Science],
Department of Math and Computer Science, Northwest Nazarene University, 623 S University Blvd, Nampa, ID 83686

Mikhail Bowerman,
Department of Math and Computer Science, Northwest Nazarene University, 623 S University Blvd, Nampa, ID 83686

Jason Colwell, Ph.D. [Associate Professor of Computer Science],
Department of Math and Computer Science, Northwest Nazarene University, 623 S University Blvd, Nampa, ID 83686

Greg Donohoe, Ph.D. P.E. [Professor Emeritus],
Computer Science Department, University of Idaho, 875 Perimeter Drive MS 1010, Moscow, ID 83844

Barry Myers, Ph.D. [Professor of Computer Science]
Department of Math and Computer Science, Northwest Nazarene University, 623 S University Blvd, Nampa, ID 83686

Abstract

1.5 to 4 million hectares of land burns in wildfire across the United States each year, contributing to post-fire erosion, ecosystem degradation and loss of wildlife habitat. Unmanned Aircraft Systems (UAS) and sensor miniaturization offer a new paradigm, providing an affordable, safe, and responsive on-demand tool for monitoring fire effects at a much finer spatial resolution than is possible with current technology. Using spectroscopic analysis of a variety of live as well as combusted vegetation samples to identify the spectral separability of vegetation classes, an optimal set of spectra was selected to be utilized by machine learning classifiers. This approach allows high resolution mapping of wildland fire severity and extent.

Keywords

fire ecology; remote sensing; machine learning; image classification

1. Background

Earth’s wildlands are an important part of our home planet, providing habitat for around 6.5 million species according to the United Nations Environment Program (Mora, 2011). In the

Corresponding Author: Dale Hamilton, dhamilton@nnu.edu.

United States (US) and elsewhere, wildlands contribute to energy development, recreational and spiritual opportunities for humans, and provide irreplaceable ecosystem services including clean water, nutrient cycling, pollination, and forage and browse for animals. Large expanses of the wildlands in the US have evolved with fire and depend on periodic wildfires for health and regeneration (Aplet, 2010). Effective management of wildfire and prescribed fires is an essential critical step toward healthy and sustainable wildlands. A quantitative understanding of the relationships between fuel, fire behavior, and the effects on human development and ecosystems can help land managers develop nimble solutions to US wildfire problems.

Fire ecology enables managers to study temporary environmental changes by accounting for the pronounced change that wildland fire effects on an ecosystem. The emerging field of ecoinformatics promises to provide the methodologies and tools needed to acquire, analyze and manage the growing amounts of complex ecological data available from the immense volume of data available in very high spatial resolution imagery which can be acquired with small unmanned aircraft system (sUAS), providing actionable knowledge of the effects of wildland fire for ecosystem management.

Current methods for acquiring imagery which can be utilized for assessing fire effects rely on satellites, which in the case of Landsat have a spatial resolution of 30 meters (NASA, 2016). Monitoring Trends in Burn Severity (MTBS) is a national project within the US to map fire severity and extent from Landsat data with records going back to 1984. However, this project only maps wildland fires greater than 400 hectares in the western US and greater than 200 hectares in the eastern US (Eidenshink, 2007; Sparks, 2015). As a result, much of the body of fire history contained in fire atlases omit the spatial extent of small and moderate sized fires (Morgan, 2014). These smaller fires can account for 20 percent of the total area burned across a landscape, which is also the most ecologically diverse of the total area burned (Hamilton, 2015). Accurate historical record of fire history is necessary in order to determine departure of current fire frequency from historic fire frequency, a key metric for determining ecosystem resilience (WFLC, 2014). Current methods for image acquisition have also included the utilization of manned aircraft, but for the purposes of obtaining post fire imagery, manned aircraft is much more expensive than sUAS, costing as much as 10 times more to operate (USGS, 2015) as well as usually being prioritized as a resource on large active fires, precluding their availability to acquire post-fire imagery.

Vegetation structural characteristics that influence wildland fire effects vary at scales that are less than the 30 meter resolution data available from the Landsat satellites. The ability to acquire higher resolution ecological data at the same or smaller scale than vegetation has the potential of increasing the accuracy of remotely sensed data (Holden, 2010). Pixels are the smallest unit that can be addressed in an image, each pixel containing a single value for each band in the image (Chang, 2016). Higher resolution images contain greater pixel density for a given area while lower resolution images utilize fewer pixels to represent the same area. Higher resolution enables objects to be represented spatially by multiple pixels, which collectively contain the spatial extent of the object (Chuvieco, 2016). Lower resolution satellite imagery pixels will commonly contain multiple heterogeneous objects, with the spectral reflectance of the pixel being influenced by each of the objects within the spatial

extent of the pixel (Sridharan, 2013). The combined spatial reflectance from the heterogeneous objects will cause the resulting pixel value to contain an aggregate value which may not adequately depict any of the objects within the pixel's spatial extent.

2. Remote Sensing with sUAS

The proliferation of small unmanned aircraft system technology has made the procurement and use of remotely sensed data a viable possibility for many organizations that could not afford to obtain such data in the past. Knowledge imparted by tools and methods being developed through this effort will enable wildland managers to establish data-informed strategies for recovery of burned areas. After a wildland fire has been suppressed, sUAS with an attached multispectral or hyperspectral image acquisition unit can enable wildland managers to obtain fire effects information in a timely, safe, and cost-effective manner. Unlike manned aircraft or satellites, sUAS can be deployed at nearly any time or location, including adverse conditions or topography where human life would be at risk, enabling a cost effective and timely method for mapping both the extent of the fire and severity of the burned area. These data can be utilized in developing the recovery plan for the fire impacted area and updating existing spatial data to reflect the current state of the vegetation and fuels within the fire perimeter.

2.1. Spatial Resolution

Current regulations by the US Federal Aviation Administration require that sUAS in the US must be flown at altitudes not exceeding 120 meters (400 ft) above ground level (AGL). Flying at such low altitudes ensures that sUAS acquired imagery will be hyperspatial, that is, where the pixel size is smaller than individual objects in the image (Sridharan, 2013). Commonly, hyperspatial (sub-decimeter) imagery allows the acquisition of very small, but ecologically significant features such as white ash (Kokaly, 2007). The presence of increased amounts of white ash has been found to be significantly correlated with increased surface fuel consumption, providing an indication of high fire severity (Hudak, 2013).

The DJI Phantom 4, a commonly available sUAS comes with a digital camera that has a horizontal field of view of 94 degrees, acquires twelve megapixel images with 3000 rows by 4000 columns of pixels. Aerial imagery acquired by a Phantom 4 while flying at an altitude of 120 meters AGL has a spatial resolution of 6.4 centimeters per pixel. Objects that are wider than that pixel resolution will be discernible in the acquired hyperspatial imagery as shown in Figure 1a. Black regions of the image are areas that were burned. Small lines and patches of white within the burned area are white ash from sagebrush which was fully combusted by the fire. Linear features are fire containment lines dug by a bulldozer.

Features that are easily identified in hyperspatial imagery are lost in low resolution 30 meter LANDSAT satellite imagery, being aggregated into more dominant neighboring features. Figure 1b shows the same scene as the preceding image, but resampled to 30 meter spatial resolution having 48 pixels aligned in 6 rows by 8 columns. If smaller objects need to be detected in imagery acquired by a sUAS, higher spatial resolution can be achieved by reducing the altitude of the sUAS.

2.2. Spectral Resolution

Machine learning based analytics use spectral reflectance to identify a variety of classes of vegetative features in images from which actionable knowledge can be derived. Spectral responses between 300 and 2500 nanometers (nm) can be used to differentiate between different image features such as white and black ash (Lentil, 2006) as well as other features of interest to fire managers such as bare earth and vegetation type (Rango, 2009). Development of analytics which can examine hyperspectral imagery will allow utilization of individual spectra as small as 10nm which offer the most information for extraction of classes of interest for fire ecology from sUAS data.

Most commercially available sUAS can be equipped to take aerial imagery with an onboard digital camera, a multi-spectral sensor with three bands capturing visible light in the blue, green and red spectrum ranging from 400 nm to 700 nm (Lebourgeois, 2008). More recently, miniaturization of hyperspectral sensors has enabled them to be carried onboard small sUAS, offering a more affordable and accessible means by which to acquire hyperspectral aerial imagery.

3. Spectroscopy

In order to establish whether classes of interest in mapping wildland fire severity are adequately distinct to enable machine learning analytics to distinguish between the classes, it was necessary to acquire a spectral library with which we established class spectral separability. Our research efforts include mapping of wildland fires in a variety of ecosystem types common to the interior northwestern US. Consequently, we found it necessary to build a spectral library in order to assure our spectroscopic analysis consisted of samples of burned and unburned vegetation common to our study region.

3.1. Vegetation Collection

In building a spectral library suitable for our spectroscopic analysis for wildland fire, it was necessary to collect both burned and unburned vegetative samples of species common to the northwestern US. This necessitated the inclusion of a biologic distribution of species across the four life forms of interest (conifer, deciduous, shrub and herbaceous) as well as both white and black ash. Collection of biologically diverse samples for inclusion in the library was facilitated by the close proximity of our research team located in Nampa, Idaho, USA to ecologically diverse ecosystems across montane southern Idaho, ranging from the xeric Owyhee Mountains to the mesic upper Payette River watershed.

3.1.1. Collection Methods—Maintaining consistent reflectance of the samples from collection of the sample to measurement of reflectivity in our lab was critical to ensuring the integrity of our data. If vegetative samples are kept moist and refrigerated, foliar moisture can be maintained which will ensure retention of chlorophyll and resulting reflectivity for up to three days (Richardson, 2002). Toward this end, when vegetative samples were collected, the cut end of the sample was wrapped in a moist paper towel and the sample was placed in a plastic bag as soon as possible. Additionally, the sample was refrigerated at the earliest opportunity. All vegetative samples were run through the spectrophotometer within 48 hours

of collection to ensure that the measure of reflectance remained consistent to what would be found with live uncut vegetation.

Reflectance measurements on white and black ash indicated that unlike unburned vegetation, spectral reflectance did not degrade over time, allowing for us to focus on measuring reflectance of unburned vegetative samples prior to running samples of burned organic materials which were not temporally sensitive through the spectrophotometer.

3.2. Spectrometry

Reflectance is a ratio of radiant flux emitted (radiance) to radiant flux received (irradiance) (Schaepman-Strub, 2006), which we measured with a Cary 100 UV-Vis spectrophotometer manufactured by Agilent Technologies equipped with a diffuse reflectance accessory. The spectrophotometer measured the diffuse spectral reflectance which occurs when light reflects off rough surfaces (Jewett, 2008) of the vegetation and ash samples. Resulting spectra are a measure of directional-hemispherical reflectance (Schaepman-Strub, 2006) from 190 to 900 nanometers (nm) with a resolution of one nm. In addition to measuring diffuse reflectance of both black ash and white ash samples, a variety of samples were measured for each of the life forms of interest (conifer, deciduous, shrub and herbaceous). In order to ensure biologic diversity of the samples, we collected 70 samples of a variety of species across each of the vegetation and ash classes.

When measuring the reflectance of each vegetative sample, three specimens were prepared from the sample for measurement with the spectrophotometer. A mean filter was applied to the reflectance measurements for the sample, averaging the reflectance values from the specimens into spectrum with a spectral resolution of 5 nm, thereby smoothing and reducing noise in the spectral data (Van Aardt, 2000). Each spectrum is identified by its midpoint, and that wavelength is used as the independent variable.

3.3. Spectroscopic Analysis

Analysis of spectral separability of the classes of interest for wildland fire severity involved both visualization of the data by plotting spectral mean of each class as well as utilization of the Student *T*-test to determine spectral separability between the classes by spectrum.

3.3.1. Data Visualization—To get an initial visualization of the data we had collected, we plotted results from each sample on a line graph. In order to simplify the visualization of the results, we calculated the mean reflectance along with the standard deviation for each class of interest from the spectral data of samples collected in each class. The mean reflectance as well as the standard deviation for each class was then graphed in a line plot shown in Figure 2.

Examination of the class mean reflectance shows complete spectral separation of black ash from white ash, with a minimum difference of 15 percentage points between the means at all the spectra across the entire spectral extent measured. This spectral separability between black ash and white ash will greatly assist classifiers in being able to distinguish between where the fire burned with lower severity (as evidenced by black ash) from where the fire burned with higher severity (as indicated by the existence of white ash).

Additional investigation of the mean reflectance of the classes of interest shows that there is spectral separation between the means of black ash and the vegetative classes in the visible and near infrared spectrum above 350 nm. This separation bodes well for the ability of development of machine learning classifiers to differentiate between black ash and vegetative classes utilizing spectral reflectance.

3.3.2. T-Test to Establish Class Separability—A *T*-test is a statistical hypothesis test which returns a decision as to whether samples taken from two populations show that the populations are statistically different from each other. This statistical test has been used to assess whether differences in spectral reflectance between species of trees are statistically significant. (Roberts, 2004)

T-Test Explanation and Setup.: For every sample collected, we have a spectroscopy graph, where reflectance (R) is plotted against wavelength (λ). Suppose we examine our data which has been resampled at a spectral resolution of five nm which takes the form of the 143 values

$$R_{190}, R_{195}, R_{200}, \ldots, R_{895}, R_{900}.$$

We examine this reflectance by wavelength data for the samples of both classes. For each of the 143 wavelength values 190nm,195nm,…,900nm we perform on the R-levels a T-test for the difference in mean. For each of the 143 different T-tests, the null hypothesis is that there is no significant difference between the reflectance levels of Class A (e.g. black ash) and those of Class B (e.g. white ash) – that any difference between the mean reflectance level of the samples of Class A and the mean reflectance level of the samples of Class B is due to chance. The P-value obtained is this chance – the probability of the observed difference occurring under the assumption of the null hypothesis. This P-value indicates the minimum significance level at which the null hypothesis can be rejected; that is, the minimum significance level at which we can assert that there is in fact a difference between Class A and Class B at that particular wavelength. Thus we have a collection of P-values P_{190}, P_{195}, …, P_{900} describing the minimum significance level for distinguishing Class A and Class B at the respective wavelengths, which we refer to with the notation $P(\lambda)$.

T-Test Analysis Results.: Two tailed T-tests were run to determine dissimilarity between the black ash and vegetation classes in addition to the black ash and white ash classes. $P(\lambda)$ for pairs of classes at each spectra were graphed in relation to a significance level. Spectrum where the $P(\lambda)$ curves are below the significance level, indicate spectrum where the classes are dissimilar, indicating a set of optimal spectrum for classifiers to consider when classifying pixels by spectral signature in order to most accurately determine which class the pixel belongs to.

$P(\lambda)$ for black ash and white ash remains below a significance level of 0.005 for the entire spectral extent, from 200 through 900 nm as shown in Figure 3. This indicates that across all of the spectra, we have very high confidence that white and black ash are separable, which is beneficial for utilization by classifiers for identifying low fire severity as indicated by the

existence of black ash as opposed to high fire severity as marked with the presence of white ash. The $P(\lambda)$ curve for black ash and vegetation exceeds a significance level of 0.04 in the ultra-violet spectrum (200–350 nm), but remains below the significance level for the rest of the spectral extent (350–900 nm). This shows that both the visible (390–700 nm) and the near infrared spectrum (700–900 nm) will be well suited for utilization by classifiers for spectral identification of burned pixels (as noted with the existence of black ash) from unburned vegetation.

In observing $P(\lambda)$ between canopy (conifer and deciduous) and surface (shrub and herbaceous) vegetation classes in Figure 3 we can detect separability with a significance level of 0.1 between the canopy and the surface classes in the spectra between 450 nm and 700 nm as evidenced by all the $P(\lambda)$ curves falling below a significance level of 0.1 in those spectrum. Additionally, from 525 nm to 700 nm the $P(\lambda)$ between the conifer and surface classes fall below 0.055, and the $P(\lambda)$ between deciduous and surface classes fall below 0.05 between 575 nm and 700 nm indicating higher confidence of separability within the spectra where $P(\lambda)$ is very near or below a significance level of 0.05. While these results do not show the same confidence of separability as found between the black ash and vegetation as shown in Figure 3, they still show spectral separation between the canopy and surface lifeforms within the visible spectrum.

While the $P(\lambda)$ curves between the canopy and surface fuels exceed the significance level of 0.1 for the spectrum between 700 and 900 nm, it is interesting to note that as the $P(\lambda)$ curves progress from 700 to 900 nm, they are very steadily decreasing, dropping below a significance level of .05 by 775 nm between the herbaceous and canopy classes. It would be interesting to see if a spectrophotometer with a greater spectral extent had been available whether $P(\lambda)$ would have dropped below the significance level for the canopy and shrub classes as they progressed further into the near infrared spectrum. If so, that would have indicated value in using the near infrared spectrum in differentiating between the vegetative classes of interest (Van Aardt, 2000).

3.3.3. Transformation of Hyperspectral Data to Color Channels—The spectral separation found between the classes between 450 and 700 nm is also the range color cameras are able to capture, showing promise for classifiers being able to distinguish between all the classes of interest using the red, green and blue bands available in multi-spectral color images. In order to assess the impact this data has on the prospect of using color imagery for mapping wildland fire, we resampled the hyperspectral data to the spectral sensitivity of a typical color camera in order to assess the separability of the classes from color imagery such as could be acquired with color cameras that are commonly mounted on a sUAS.

In order to derive muli-spectral data typical of color imagery from our hyperspectral data, we created a model of a typical color from the spectral sensitivity data from the cameras mentioned by Jiang (2013) which was measured at 10 nm spectral resolution. We averaged the spectral sensitivity curves of the set of cameras into a single set of sensitivity curves indicative of the spectral sensitivity of the red (570–670 nm), green (500–570 nm) and blue (420–500 nm) channels of a typical camera as shown in Figure 4. These bands from our

typical camera model (TCM) were then used to obtain a weighted average of each of our spectral samples into red, green and blue channel values that are representative of the reflectance of that species in color imagery. The mean as well as the standard deviation of the samples from each class are shown in Figure 5. The color reflectance values for the samples were then run through the *T*-tests in the same manner as mentioned previously for the hyperspectral data. Looking at the results of the *T*-tests between the classes in the color channels as shown in Figure 6, black ash shows high confidence of separability with both white ash and the vegetation samples with a significance level of 0.001 as was seen with the hyperspectral data. The vegetation classes show separability with the surface and canopy classes *P*-values dropping below a significance level of 0.05 in each of the color bands with the exception of conifer in the blue band which has separability with a *P*-value of 0.06 shrub and 0.07 with herbaceous.

4. Application

The separability between classes established with the *T*-tests shows potential for enabling the development of machine learning based analytics which utilize spectral reflectance to differentiate between ash and vegetation classes for mapping wildland fire severity and extent. In particular, the low *P*-values across the same spectra captured by common digital cameras illustrates the potential of establishing class separability with a multispectral color image containing red, green and blue bands.

In order to test the applicability of these findings, we trained machine learning classifiers developed by our team with examples of black ash, white ash and surface vegetation shown in Figure 1a. The classifier used those training examples to classify the rest of the image into unburned vegetation, low severity fire where the classifier detected black ash and high severity fire as evidenced by the existence of white ash. Our analytics then utilized image processing tools we developed to clear up the resulting fire severity image by performing object enhancement, edge smoothing and noise reduction utilizing common morphological algorithms. The resulting fire severity image is shown in Figure 7 where:

- black indicates pixels the classifier labeled as unburned vegetation
- grey corresponds to areas that burned with a low intensity as evidenced by the existence of black ash
- white corresponds to spots that burned with high intensity as evidenced by white ash that resulted from fully combusted sagebrush

5. Conclusion

The *T*-test results show good class separability in the visible spectrum between black ash, white ash, the canopy vegetation as well as the surface vegetation classes. Additionally, the near infrared spectrum also shows promise for class separability between white ash, black ash and the vegetation classes. The *P*-values above 750 nm indicate spectral separability between the canopy and herbaceous vegetation classes in the near-infrared spectrum. The *P*-value trends between the canopy and shrub vegetation class approaching the upper bound of the spectral extent of this study indicate the potential of separability between the canopy and

shrub vegetation classes further into the infrared spectra past the spectrum measured by our spectrophotometer. The *T*-test results did not show good intra-class separability in the ultraviolet spectra below 450 nm.

Class separability found in the visible and infrared spectrum can be utilized in the development of machine learning analytics by identifying and utilizing only spectra that provide good separability between classes, thereby excluding spectra that do not provide information as to class separability. The class separability we found in the near infrared spectrum indicate that there would be benefit to using a sensor that can record spectral reflectance both in the visible and the near infrared spectrum, particularly if the spectral extent of the sensor extends past 900 nm. The $P(\lambda)$ trends we observed between the canopy and surface vegetation classes approaching 900 nm continued further into the near infrared spectrum, again establishing separability between the canopy and surface vegetation classes further into the near infrared spectrum.

Determination of spectral separability was found between all the classes of interest for mapping wildland fire severity in the visible spectra (450–700 nm). This separation was found both with hyperspectral data (Figure 3) as well as multi-spectral color data (Figure 6) transformed from the hyperspectral data using the TCM. These results show promise for being able to map wildland fire severity using the color digital cameras that come stock on many sUAS, as they detect reflected light in three bands covering that same 450 to 700 nm spectra (Chang, 2016).

Our data and analysis indicate that an ordinary three-band color camera will provide enough information. The additional spectral resolution (about 20 nm per band) provided by a hyperspectral imager does not seem to provide enough additional relevant information to justify the cost of the instrument and the added computational burden to exploit that information. There may be potential use for a hyperspectral sensor in the longer wavelengths of the near infrared spectrum (900–5000 nm) due to the variation across smaller spectrum in that range, where it appears that the $P(\lambda)$ curves may drop below the significance level (Van Aardt, 2000). However, our study did not explore this spectral range.

5.1. Future Work

This effort was part of a larger ongoing research project at Northwest Nazarene University developing analytics for mapping wildland fire effects from hyperspatial sUAS imagery using machine learning and image processing. The goal of the research project is to enable the acquisition, analysis and management of hyper-resolution imagery for mapping burn severity in a more responsive, affordable and safe manner than is possible with current methods. This includes the development and calibration of image acquisition, processing and classification tools within our fire effects analytics, leveraging the results of these conclusions to focus the analytics on spectra with the best class separability. Current research topics being explored include:

- Post-fire image acquisition methods over wildland fire burns in montane ecosystems with varying topography and vegetation types. This effort is being conducted in cooperation with the Boise National Forest in southern Idaho, USA.

- Investigation of the applicability of image texture (Haralick, 1973) as an additional input with color image bands for improving machine learning accuracy for mapping wildland fire effects (Hamilton, 2017).
- Evaluation of the ability of increased spatial resolution to improve mapping of wildland fire effects by assessing machine learning accuracy when using hyperspatial (sub-decimeter) as opposed to low resolution (30 meter) imagery.
- Assessment of a variety of machine learning algorithms for mapping wildland fire effects. Algorithms currently being evaluated include Support Vector Machines, k-Nearest Neighbor, Artificial Neural Networks and Decision Trees.

While the results of the analysis described are promising for class separability in the visible spectrum, additional research is needed looking at class spectral reflectance in the near and shortwave infrared spectrum which could not be measured by the spectrophotometer that was available. Near and shortwave infrared have been shown to hold promise for wildland vegetation species identification, (Van Aardt, 2000), fire severity mapping (Lentile, 2006) and vegetation health (Lasaponara, 2006). This warrants further investigation of the utilization of those spectra for establishment of class separability for hyper-resolution mapping of wildland fire severity.

Acknowledgements

We would like to acknowledge Sarah Hurt, Field Botanist with the Deer Flat National Wildlife Refuge for assisting with collection of vegetation samples and spectronomy. Additionally, we acknowledge Jerry Harris for his assistance in incorporating the spectrophotometer into our research. We would also like to acknowledge Leslie Hamilton for editing and review of this manuscript.

References

Aplet GH, & Wilmer B (2010). Potential for restoring fire-adapted ecosystems: Exploring opportunities to expand the use of wildfire as a natural change agent. Fire Management Today, 70(1), 35–39.

Chang Kang-Tsung. 2016 Introduction to geographic information systems Eighth edition. ed. New York, NY : McGraw-Hill Education,.

Chuvieco Emilio. 2016 Fundamentals of satellite remote sensing: An environmental approach CRC Press.

Eidenshink Jeffery C., Schwind Brian, Brewer Ken, Zhu Zhu-Liang, Quayle Brad, and Howard Stephen M. 2007 A project for monitoring trends in burn severity. Fire Ecology 3 (1): 3–21.

Jewett JW, and Serway RA 2008 Physics for scientists and engineers with modern physics Cengage Learning EMEA.

Hamilton D, and Hann W 2015 Mapping landscape fire frequency for fire regime condition class. Paper presented at Large Fire Conference, Missoula, MT.

Hamilton D, Branham J, and Myers B 2017 Evaluation of Texture as an Input of Spatial Context for Machine Learning Mapping of Wildland Fire Effects. Manuscript submitted for publication in the Proceedings of ACM SIGSPATIAL 2017.

Haralick R, and Shanmugam K 1973 Textural features for image classification. IEEE transactions on systems, man, and cybernetics 610–621

Holden Zachary A., Penelope Morgan, Alistair MS Smith, and Lee Vierling. 2010 Beyond landsat: A comparison of four satellite sensors for detecting burn severity in ponderosa pine forests of the Gila Wilderness, NM, USA. International Journal of Wildland Fire 19 (4): 449–58.

Hudak Andrew T., Ottmar Roger D., Vihnanek Robert E., Brewer Nolan W., Smith Alistair MS, and Morgan Penelope. 2013 The relationship of post-fire white ash cover to surface fuel consumption. International Journal of Wildland Fire 22 (6): 780–5.

Kokaly Raymond F., Rockwell Barnaby W., Haire Sandra L., and King Trude VV. 2007 Characterization of post-fire surface cover, soils, and burn severity at the Cerro Grande Fire, New Mexico, using hyperspectral and multispectral remote sensing. Remote Sensing of Environment 106 (3): 305–25.

Lasaponara R 2006 Estimating spectral separability of satellite derived parameters for burned areas mapping in the calabria region by using SPOT-vegetation data. Ecological Modelling 196 (1): 265–70.

Lebourgeois Valentine, Agnès Bégué Sylvain Labbé, Mallavan Benjamin, Prévot Laurent, and Roux Bruno. 2008 Can commercial digital cameras be used as multispectral sensors? A crop monitoring test. Sensors 8 (11): 7300–22. [PubMed: 27873930]

Lentile Leigh B., Holden Zachary A., Alistair MS Smith Michael J. Falkowski, Hudak Andrew T., Morgan Penelope, Lewis Sarah A., Gessler Paul E., and Benson Nate C. 2006 Remote sensing techniques to assess active fire characteristics and post-fire effects. International Journal of Wildland Fire 15 (3): 319–45.

Mora Camilo, Tittensor Derek P., Adl Sina, Simpson Alastair GB, and Worm Boris. 2011 How many species are there on earth and in the ocean? PLoS Biol 9 (8): e1001127. [PubMed: 21886479]

Morgan P, Heyerdahl E, Miller C, Wilson A, and Gibson C 2014 Northern Rockies Pyrogeography: An example of fire atlas utility. Fire Ecology 10 (1): 14.

National Aeronautics and Space Administration. What are the band designations for the Landsat satellites? Available from http://landsat.usgs.gov/band_designations_landsat_satellites.php (accessed 7/21/2016).

Rango Albert, Laliberte Andrea, Herrick Jeffrey E., Winters Craig, Havstad Kris, Steele Caiti, and Browning Dawn. 2009 Unmanned aerial vehicle-based remote sensing for rangeland assessment, monitoring, and management. Journal of Applied Remote Sensing 3 (1): 033542,033542-15.

Richardson AD, and Berlyn GP 2002 Changes in foliar spectral reflectance and chlorophyll fluorescence of four temperate species following branch cutting. Tree Physiology 22 (7) (5): 499–506. [PubMed: 11986053]

Roberts Dar A., Ustin Susan L., Ogunjemiyo Segun, Greenberg Jonathan, Dobrowski Solomon Z., Chen Jiquan, and Hinckley Thomas M. 2004 Spectral and structural measures of northwest forest vegetation at leaf to landscape scales. Ecosystems 7 (5): 545–62.

Schaepman-Strub G, Schaepman M, Painter T, Dangel S, & Martonchik J (2006). Reflectance quantities in optical remote sensing—Definitions and case studies. Remote Sensing of Environment, 103(1), 27–42.

Sparks Aaron M., Boschetti Luigi, Alistair MS Smith Wade T. Tinkham, Lannom Karen O., and Newingham Beth A. 2015 An accuracy assessment of the MTBS burned area product for shrub–steppe fires in the northern great basin, United States. International Journal of Wildland Fire 24 (1): 70–8.

Sridharan H, and Qiu F 2013 Developing an object-based hyperspatial image classifier with a case study using WorldView-2 data. Photogrammetric Engineering & Remote Sensing 79 (11) (11 2013): 1027–36.

Aardt Van, Jan AN. 2000 Spectral Separability among Six Southern Tree Species

Wildland Fire Leadership Council. 2014 National Cohesive Wildland Fire Management Strategy http://www.forestsandrangelands.gov

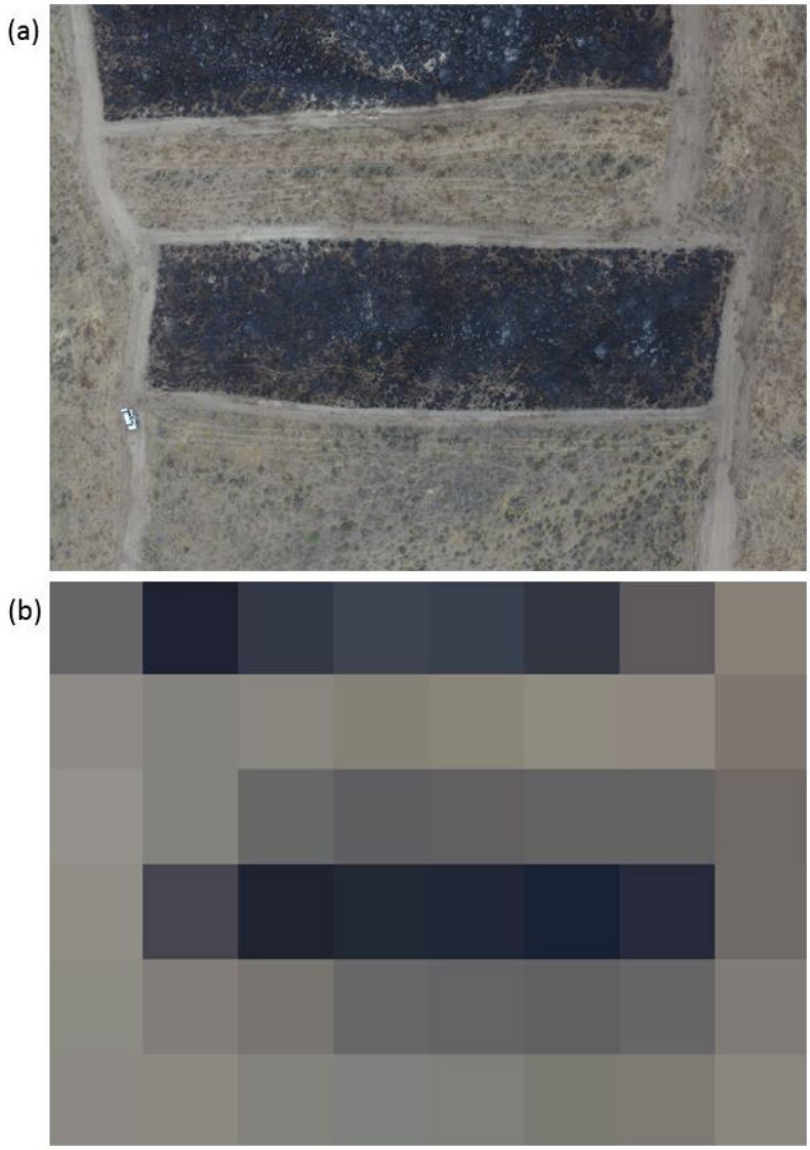

Figure 1 –.

(a) Image of a rangeland study area acquired with a Phantom 3 Professional sUAS flying at 120 meters AGL with a spatial resolution of 6.4 centimeters per pixel. (b) Same scene resampled to 30 meter resolution with six rows and eight columns of pixels.

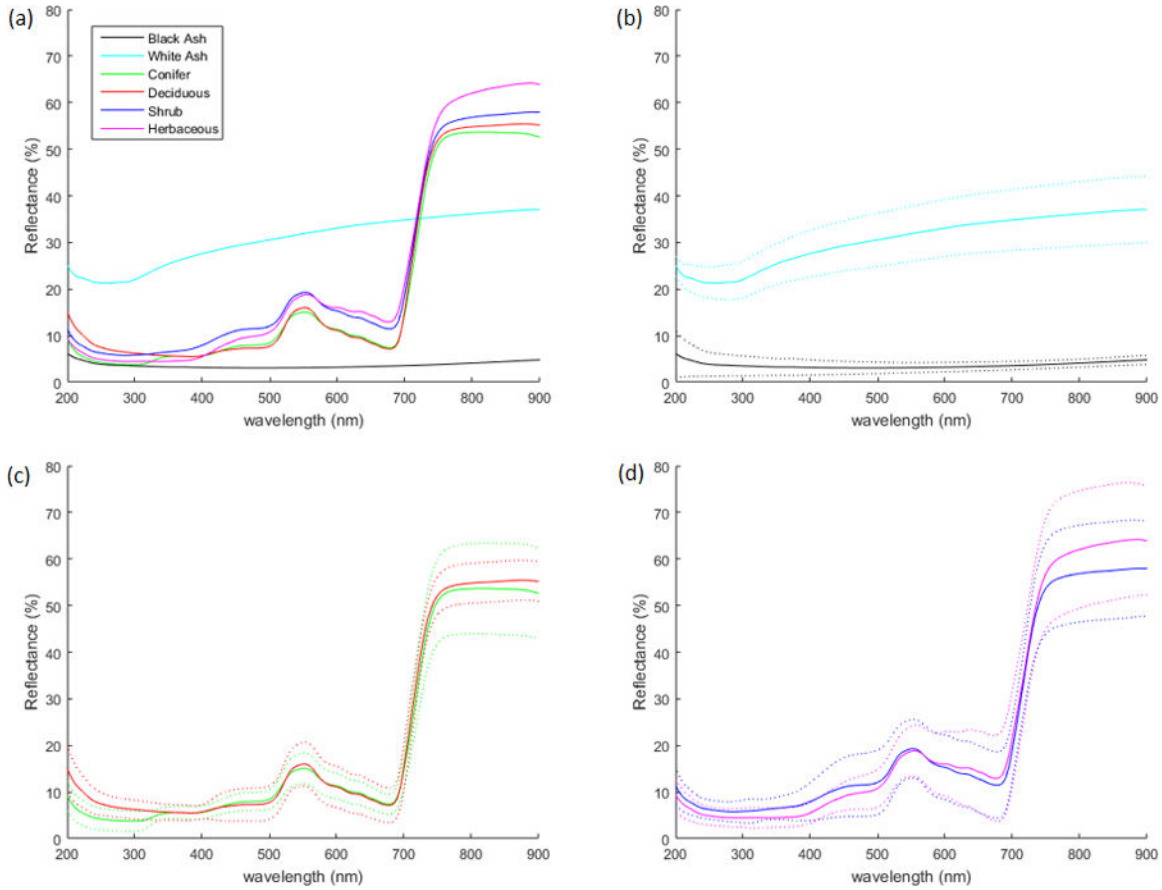

Figure 2 –.

(a) Mean reflectance for black ash, white ash, conifer, deciduous, shrub, and herbaceous. (b) Mean reflectance for black and white ash (solid line) with plus and minus one standard deviation (dotted lines). (c) Mean reflectance for canopy lifeforms (conifer and deciduous) with plus and minus one standard deviation. (d) Mean reflectance for surface lifeforms (herbaceous and shrub) with plus and minus one standard deviation.

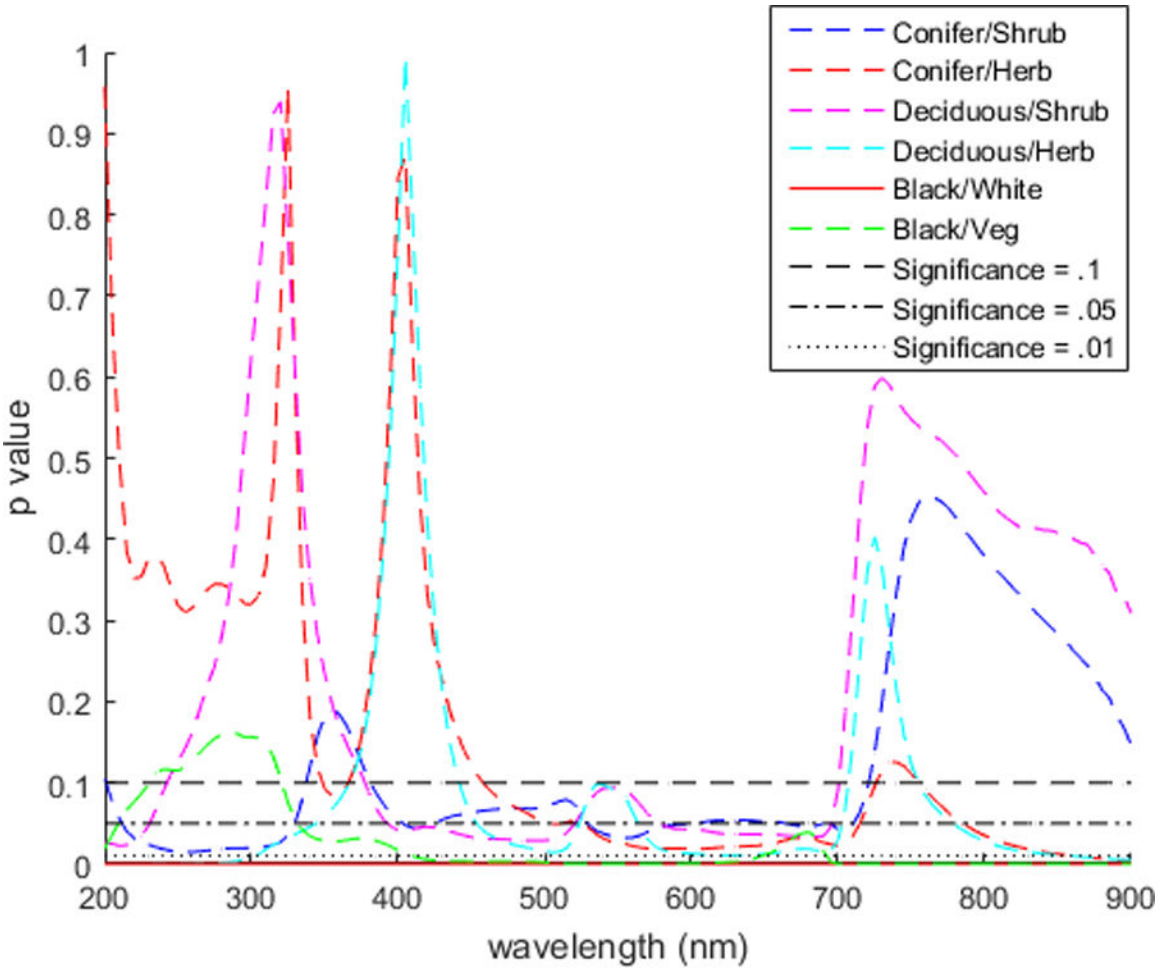

Figure 3 –.

Burn severity image showing unburned vegetation (black), low intensity burn (grey) and high severity burn (white).

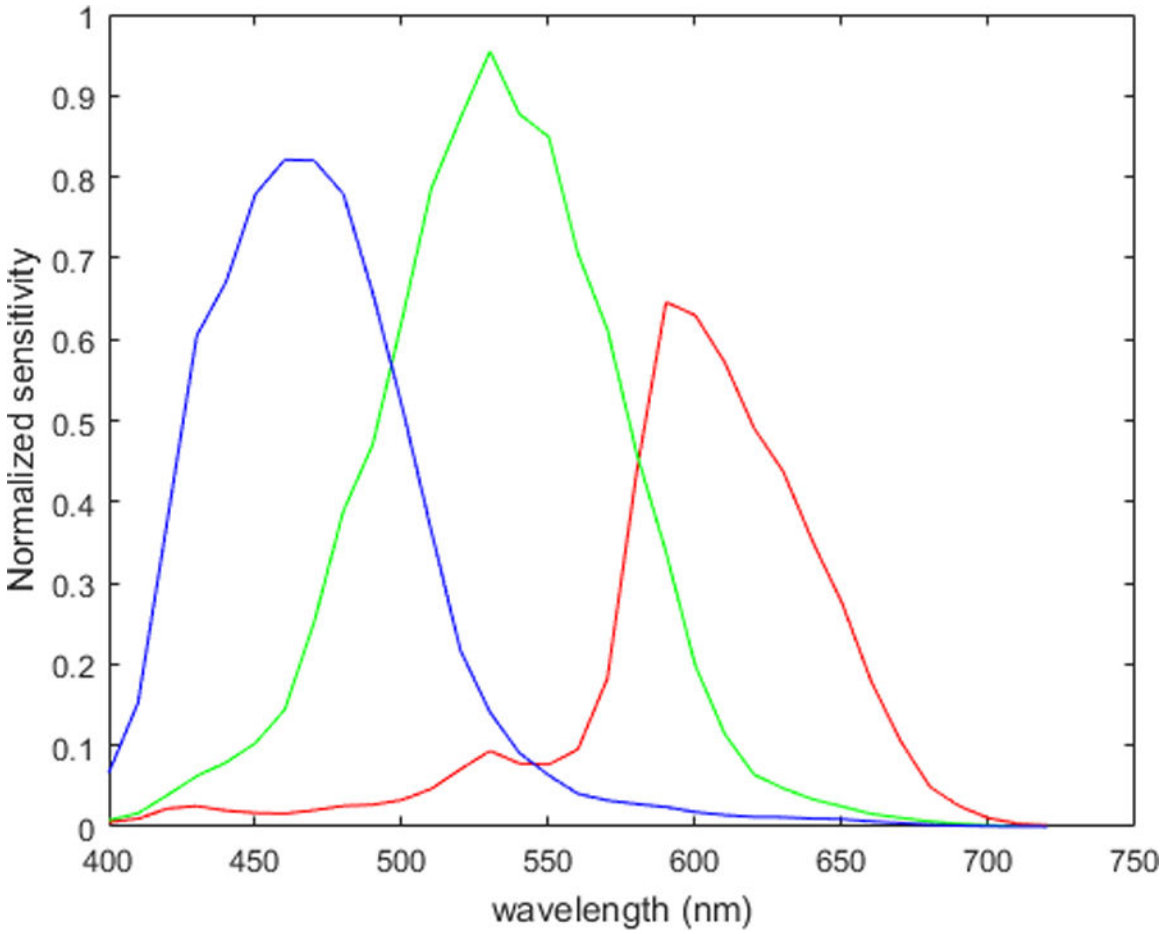

Figure 4 –.
Typical camera model spectral sensitivity curves for red, green and blue channels.

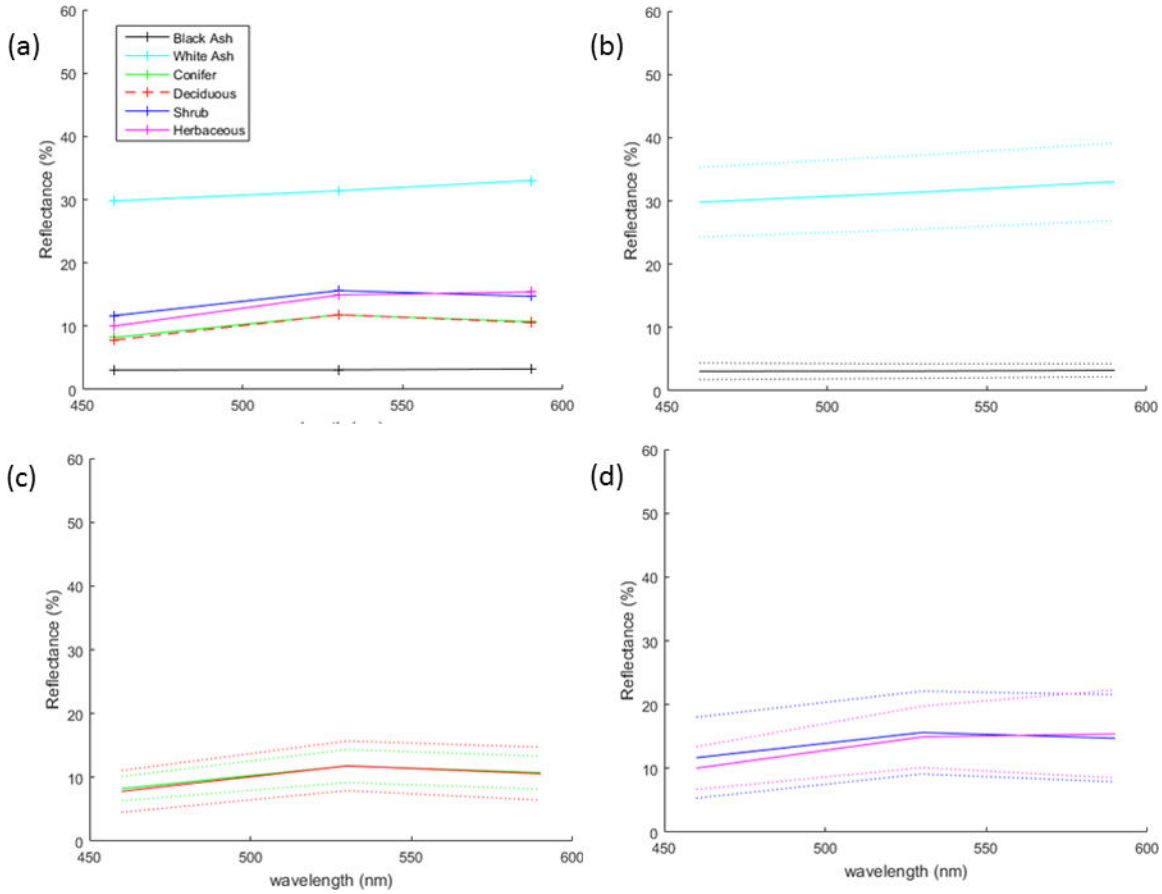

Figure 5 –.

(a) Mean reflectance in red, green and blue channels of the TCM for black ash, white ash, conifer, deciduous, shrub, and herbaceous classes. TCM channels are centered on the wavelength with the peak spectral sensitivity of the corresponding TCM channel. (b) Mean reflectance for black and white ash (solid line) with plus and minus one standard deviation (dotted lines). (c) Mean reflectance for canopy lifeforms (conifer and deciduous) with plus and minus one standard deviation. (d) Mean reflectance for surface lifeforms (herbaceous and shrub) with plus and minus one standard deviation.

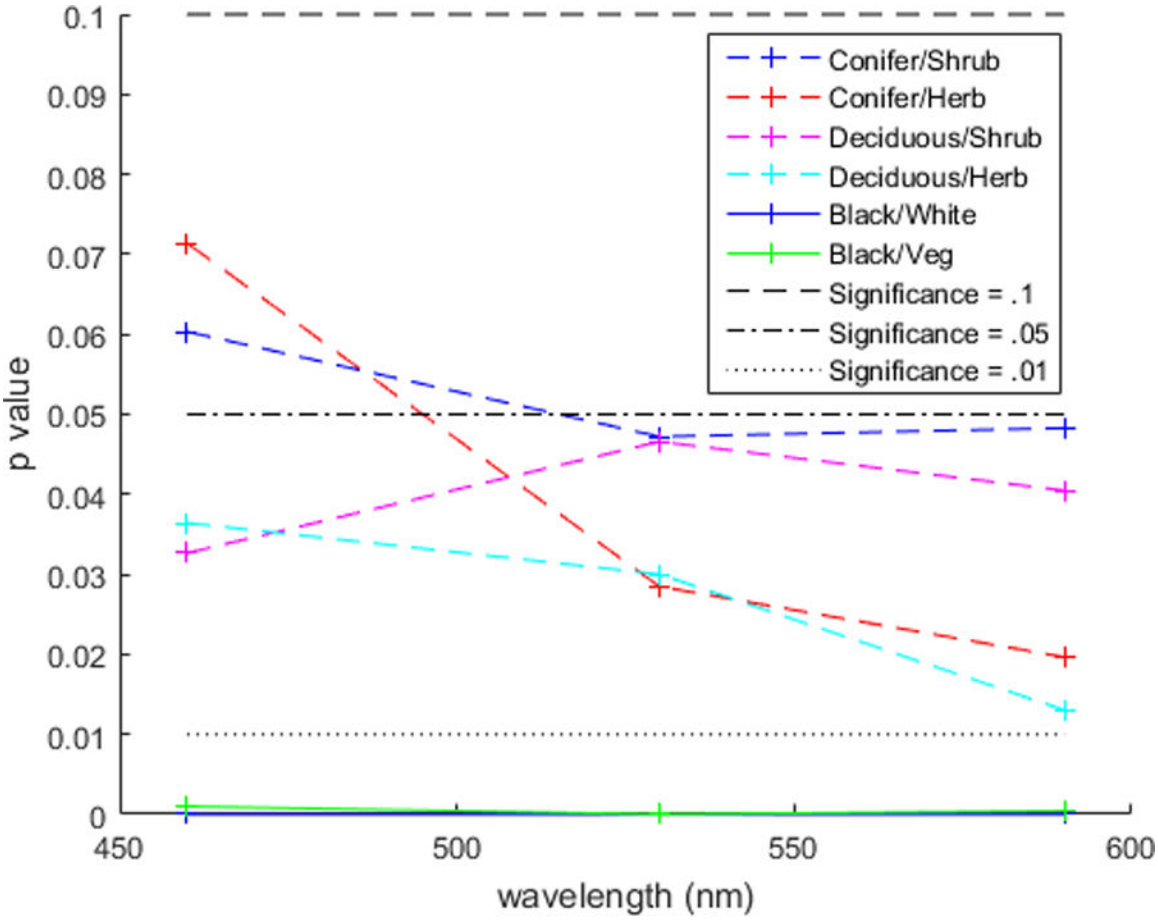

Figure 6 –.
T-test results for classes of color band reflectance as modeled from the TCM.

Figure 7 –.

Burn severity raster generated by machine learning classifier from image in Figure 1a. Black indicates unburned vegetation, grey corresponds to low intensity as evidenced by the existence of black ash and white represents spots that burned with high intensity as evidenced by white ash.